NASA TECHNICAL MEMORANDUM

NASA TM X-52900

NASA TM X-52900

RELIABILITY TESTING AND DEMONSTRATION
SESSIONS IV C, E

by Vincent R. Lalli
Lewis Research Center
Cleveland, Ohio

Lecture Notes for Eighth Annual Reliability Engineering and Management Institute sponsored by the University of Arizona
Tucson, Arizona, November 2-11, 1970

RELIABILITY TESTING AND DEMONSTRATION SESSIONS IV C,E

by Vincent R. Lalli

National Aeronautics and Space Administration
Lewis Research Center
Cleveland, Ohio

INTRODUCTION

The outline shown below describes the material that will be covered in the Reliability Testing and Demonstration Lectures IV C,E:

IV B. Application of Statistical Methods

1. Testing with normal units
2. Determination of confidence limits
3. Testing with lognormal units
4. Determination of confidence limits
5. Testing with bionomial and Poisson events
6. Determination of confidence limits

IV E. Reliability Program Case History

1. SERT II Reliability engineering
2. Reliability stress analysis of a microthruster power conditioner

A great deal of work has been done by various researchers to develop mathematical concepts suitable for reliability studies. The interested reader should consult References 1 through 4 for additional details pertaining to statistical methods for discrete and continuous random variables.

E-4587

In these notes effort will be concentrated on four functions: (1) Failure, f(t); (2) Reliability, R(t); Failure rate, λ; and (4) Hazard rate, λ'. Since it is usually important to know how well a point estimate has been defined, some consideration will be given to calculation of confidence limits for normal, lognormal, bionomial and Poisson functions. These notes consider specific cases to show how analytical or graphical statistical methods can be used in summarizing test data.

1. Testing with normal units (analytical procedure)

A mechanical part is being used where friction, mechanical loading and temperature are the principal failure causing stresses. Assume that tests to failure have been conducted for these mechanical parts resulting in the data shown in table I.

(a) Calculate the mean-time-between-failures and standard deviation.

(b) What are the hazard rate at 85.3 K hours and failure rate during the next 10.3 K hour interval?

(c) What are the failure and reliability time functions?

The mean-time-between-failures and standard deviation can be calculated for the data given in table I as follows:

$$(a)\ \bar{t} = \frac{\sum_{f=1}^{n} t_f}{n}$$

where

$\bar{t}$ mean-time-between-failures, hr

t_f time-to-failure, hr

n number of observations

therefore, using the data from table I

$$\bar{t} = \frac{750\ K}{10} = 75\ K \text{ hours}$$

and

$$\sigma = \left[\frac{\sum_{f=1}^{n} t_f^2 - \frac{\left(\sum_{f=1}^{n} t_f \right)^2}{n}}{n - 1} \right]^{1/2}$$

where σ = unbiased standard deviation

$$\left(\sum_{f=1}^{n} t_f^2 \right) = 5.7213 \times 10^4 (K\ hr)^2 \text{ column 3, table I,}$$

$$\left(\sum_{f=1}^{n} t_f \right)^2 = (7.5 \times 10^2)^2 = 5.625 \times 10^5\ (K\ hr)^2$$

Therefore,

$$\sigma = \left(\frac{57213 - 56250}{9}\right)^{1/2} = \left(\frac{963}{9}\right)^{1/2} = 10.3 \text{ K hr}$$

(b) The hazard rate, λ' and failure rate λ are calculated as follows:

$$\lambda' = \frac{\text{normal ordinate at } 85.3 \text{ K hr}}{\text{normal area } 85.3 \text{ K hr to } \infty}$$

Let $\bar{Y}_1$ = normal ordinate at 85.3 K hr

Z_1 = standardized normal variable

$$= \frac{t - \bar{t}}{\sigma} = \frac{(85.3 - 75.0) \text{ K hr}}{10.3 \text{ K hr}} = +1.0$$

Table 4 (p. 352 of ref. 5) for $Z = +1.0$ gives $\bar{Y}_1 = 0.242$. The scale constant K_s for this problem is:

$$K_s = \frac{n\theta}{\sigma}$$

where θ = class interval

$$Y_1 = f(t_1) = K_s \bar{Y}_1 = \frac{10 \text{ x } 1 \text{ F}}{10.3 \text{ K hr}} \text{ x } 0.242 = 2.35 \text{x} 10^{-4} \text{ F/hr}$$

Let $R(t_1)$ = normal area 85.3 hr to ∞. From table 3 (p. 351 of ref. 5) for $Z_1 = +1.0$

$Q(t_1) = 0.841$ area from $-\infty$ to Z_1

Since $Q(t_1) + R(t_1) = 1.000$

$$R(t_1) = 1.000 - 0.841 = 0.159$$

$$\lambda' = \frac{2.35\text{x}10^{-4}\ \text{F/hr}}{1.59\text{x}10^{-1}} = 1.47\text{x}10^{-3}\ \text{Failures/hr}$$

and

$$\lambda = \frac{1}{h}\left[1 - \frac{R(t_2)}{R(t_1)}\right] \qquad h = 10.3\ \text{K hr}$$

$R(t_2)$ = normal area 95.6 K hr to ∞

$$Z_2 = \frac{(95.6 - 75.0)\ \text{K hr}}{10.3\ \text{K hr}} = +2.0$$

From table 3, $Q(t_2) = 0.977$ and $R(t_2) = 0.023$

$$\lambda = \frac{1}{10.3\ \text{K hr}}\left(1 - \frac{0.023}{0.159}\right) = \frac{8.56\text{x}10^{-1}}{1.03\text{x}10^{4}} = 8.31\text{x}10^{-5}\ \text{Failures/hr}$$

(c) The constants for $f(t)$ and $R(t)$ are calculated as follows:

$$\frac{1}{\sigma\sqrt{2\pi}} = \frac{1}{1.03\text{x}10^{4} \times 2.52} = 3.87\text{x}10^{-5}$$

$$2\sigma^2 = 2 \times (1.03\text{x}10^{4})^2 = 2.12\text{x}10^{8}$$

Therefore,

$$f(t) = 3.87\text{x}10^{-5}\ e^{-(t-7.5\text{x}10^{4})^2/2.12\text{x}10^{8}}$$

$$R(t) = 3.87\text{x}10^{-5} \int_{t}^{\infty} e^{-(t-7.5\text{x}10^{4})^{2}/2.12\text{x}10^{8}}\, dt$$

2. Determination of parameters and confidence limits

Twenty-five (25) mechanical parts have been tested to failure. The mean-time-between failures has been calculated to be 75 K hours with σ = 10.3 K hours (see problem 1). (a) What are the upper and lower confidence limits at a 90 percent confidence level?

The upper and lower confidence limits are given by:

$$U = \bar{t} + K_{\alpha/2} \frac{\sigma}{\sqrt{n}}$$

$$L = \bar{t} - K_{\alpha/2} \frac{\sigma}{\sqrt{n}}$$

where

$\bar{t}$	mean-time-between failures, hr
$K_{\alpha/2}$	normal coefficient
σ	unbiased standard deviation, hr
n	number of samples
$\frac{\alpha}{2}$	area under one tail

For this problem:

$1 - \alpha = 0.90$ $\quad \alpha = 0.10$ $\quad \frac{\alpha}{2} = 0.05$

$K_{\alpha/2} = 1.64$ from table 3 of reference 5

$$U = 75\ K + \frac{1.64 \times 10.3\ K}{\sqrt{25}} = 78.4\ K\ hr$$

$$L = 75\ K - \frac{1.64 \times 10.3\ K}{\sqrt{25}} = 71.6\ K\ hr$$

This means that 90 percent of the time the mean-time-between-failures estimate $\bar{t}$ for problem 1 with a larger sample size will be between 71 600 and 78 400 hours. It should be noted that the sample size for problem 1 was only 10 parts. If possible, try to keep $n \geq 25$ for estimating normal parameters with the above equations.

If the sample size, $n < 25$ then use should be made of the student's t distribution (see ref. 6). If problem 2 is reworked for a smaller sample size of 10, it will be interesting to see the effect that sample size has on the size of confidence intervals.

$$U = \bar{t} + t_{\alpha} \frac{s}{\sqrt{n}}$$

$$L = \bar{t} - t_{\alpha} \frac{s}{\sqrt{n}}$$

where

t_{α} student t coefficient

s standard deviation, hr

For this case with $\alpha = 0.10$, $\nu = n - 1 = 10 - 1 = 9$

t_α = 1.83 from table IV of reference 6, page 243

$$s = \left(\frac{57213 - 56250}{10}\right)^{1/2} = 9.82 \text{ K hr}$$

$$U = 75 \text{ K hr} + \frac{1.83 \times 9.82 \text{ K hr}}{\sqrt{10}} = 80.7 \text{ K hr}$$

$$L = 75 \text{ K hr} - \frac{1.83 \times 9.82 \text{ K hr}}{\sqrt{10}} = 69.3 \text{ K hr}$$

It will be noted that the smaller sample size gives a larger interval of uncertainty for $\overline{t}$.

3. Testing with lognormal units (graphical procedure)

A cable used as guy supports for sail experiments in wind tunnel testing exhibited the time-to-failure performance data given in table II.

(a) Write the failure and reliability functions.

(b) What is the hazard rate at 5715 hours?

(c) what is the failure rate during the next 3000 hours?

a. The essential steps for solving this problem are given below:

(1) Table II gives the median rank for each ordered position.

(2) Plot on lognormal probability graph paper (probability x 2 log cycles) median ranks against failure age as shown in figure 1.

(3) If a straight line can be fit to these plotted points, then the time-to-failure function is lognormal.

(4) The mean-time-between-failures is calculated by $\overline{t}' = \log_e(\overline{t})$ where $\overline{t}$ = 6970 hours as shown in figure 1 for a median ranks of 50 percent, hence $\overline{t}'$ = 8.84.

(5) The standard deviation is calculated by

$$\sigma_{t'} = \left[\frac{\log_e t_U - \log_e t_L}{3}\right]$$

where t_U = 49 500 hours and t_L = 1020 hours as shown in figure 1 for a median and [1 - rank] of 93.3 percent; hence

$$\sigma_{t'} = \left[\frac{10.8 - 6.93}{3}\right] = 1.29.$$

Using these constants the expressions for $f(t)$ and $R(t)$ can be obtained.

$$f(t) = \frac{3.07\text{x}10^{-1}}{t}\, e^{-(t'-8.84)^2/3.32}$$

$$R(t) = 3.07\text{x}10^{-1} \int_{\log_e(t)}^{\infty} e^{-(t'-8.84)^2/3.32}\, dt$$

b. The lognormal ordinate required for λ' can be calculated as follows:

$$Z_2 = \left(\frac{t' - \bar{t}'}{\sigma_{t'}}\right) = \left(\frac{8.66 - 8.84}{1.29}\right) = -0.139$$

$\bar{Y}_2$ = 0.395 from table 4 of reference 5

$$Y_2 = \frac{N\bar{Y}_2}{\sigma_{t'}} = \frac{10 \text{ x } 0.395}{1.29} = 3.06$$

$$f(t') = \frac{Y_2}{t} \quad \frac{3.06}{5.715\text{x}10^3} = 5.34\text{x}10^{-4} \text{ Failures/hr}$$

The lognormal area from t' to infinity can be obtained directly from figure 1 using the [1 - rank] scale. Enter the time-to-failure ttf ordinate at 5715 hours; project over to the lognormal life function $Q(t)$ and down to the [1 - rank] abscissa value of 0.638. Therefore the hazard rate λ' at 5715 hours is:

$$\lambda' = \frac{5.34 \times 10^{-4}}{6.38 \times 10^{-1}} = 8.36 \times 10^{-4} \text{ Failures/hr}$$

c. The failure rate during the next 3000 hours is calculated knowing the $R(t_1) = 0.638$ at ttf = 5715 hours and obtaining $R(t_2) = 0.437$ from figure 1 at ttf = 8715 hours. Therefore,

$$\lambda = \frac{1}{3 \times 10^{3}} \left(1 - \frac{0.437}{0.638}\right) = 1.05 \times 10^{-4} \text{ Failures/hr}$$

4. Determination of confidence limits

It has been shown that the guy supports of problem 3 exhibited a reliability of 0.638 at a ttf of 5715 hours. Consider now the procedure for determining the confidence band on this lognormal estimate. The data needed for the graphical construction of the 90 percent confidence lines on the lognormal graph of figure 1 is also given in table II. The steps necessary to graphically construct the confidence lines in figure 1 are as follows:

(1) Enter the ranks axis with the first 5 percent rank value hitting $Q(t)$ the lognormal life function shown in figure 1; ordered sample number 3, 5 percent rank 8.7.

(2) Draw a vertical line to intersect $Q(t)$ at point 1 as shown in figure 1.

(3) Draw a horizontal line to cross the corresponding median rank; ordered sample number 3, median rank 25.9.

(4) The intersection point (point 2 in fig. 1) of step 3 and the median rank line is one point on the 95 percent confidence line.

(5) Repeat steps 1 through 4 until the desired time-to-failure is covered, 5715 hours in this case.

(6) The 5 percent confidence line is obtained in a similar manner. Enter the ranks axis with the 95 percent failure rank, 25.9 for ordered sample number 1.

(7) Draw a vertical line which intersects $Q(t)$ at point 3.

(8) Draw a horizontal line to cross the corresponding median rank; ordered sample number 1, median rank 6.7.

(9) The intersection point (point 4 in fig. 1) of these two lines is one point on the 5 percent confidence line.

(10) Repeat steps 6 through 9 until the desired time-to-failure is covered.

At 5715 hours the 90 percent confidence interval for $Q(t)$ is from figure 1: 19.7 percent, 69.4 percent. Hence, a 90 percent confidence interval for $R(t)$ at 5715 hours is 0.803 to 0.306. Incidentally, this graphical procedure for finding confidence intervals is completely general and can be used on other types of life test diagrams.

5. Testing with the binomial and Poisson events

The binomial and Poisson distributions are discrete functions of the number of failures N_f which occur rather than time t. A summary of these frequency functions is given in figure 1 of reference 4.

A suspicious lot of explosive bolts is estimated to be 15 percent defective due to improper loading density observed in neutron radiography.

(a) Calculate the probability of one defective unit appearing in a flight quantity of four.

(b) Plot the resulting histogram.

(c) What is the reliability from the first defect?

Not much failure density data is available, however, past experience with pyrotechnic devices has shown that the binomial distribution applies. From the given data:

q per unit number of effectives = 0.85

p per unit of defectives = 0.15

n sample size = 4

N_f possible number of failures = 0, 1, 2, 3, 4

The frequency functions corresponding to these constants are given below:

$$f(N_f) = \frac{n!}{(n - N_f)!\, N_f!}\, p^{N_f}\, q^{n-N_f}$$

$$f(N_f) = \frac{4!}{(4 - N_f)!\, N_f!}\, p^{N_f}\, q^{4-N_f}$$

$$R(N_f) = \sum_{j=N_f}^{n} \frac{n!}{(n - j)!\, j!}\, p^j\, q^{n-j}$$

$$R(N_f) = \sum_{j=N_f}^{4} \frac{4!}{(4 - j)!\, j!}\, p^j\, q^{n-j}$$

One easy method to obtain the binomial expansion coefficients is to make use of Pascal's triangle. Pascal found that there was symmetry to the coefficient development and explained it as shown in table III. Column 1 gives the sample size n. Column 2 gives the possible number of failures. Column 3 gives the binomial expansion coefficients. The numbers in the dashed triangle in column 3 are obtained by adding the two numbers above the number to get that number; that is, refer to dashed insertion the triangle 3 + 3 = 6. In expanded form $f(N_f)$ becomes

$$f(N_f) = q^4 + 4q^3p + 6q^2p^2 + 4qp^3 + p^4$$

The probability of one defective unit appearing in the flight quantity of 4 is given by the second term in the expansion; hence,

$$4q^3p = 4(0.85)^3(0.15) = 0.37$$

The resulting histogram for this distribution is shown in figure 2. The probability that 2, 3, or 4 defects will occur as the reliability from the first defect is the sum of the remaining terms in the binomial ex-

pansion. This probability can be calculated using the following equation:

$$R(N_f) = \sum_{j=2}^{4} \frac{4!}{(4 - j)!\ j!}\ p^j\ q^{n-j}$$

However, it is simpler to use the histogram graph and sum the probability defects over N_f from 2 to 4. Hence,

$$R(2) = 0.096 + 0.011 = 0.108$$

These explosive bolts in their present form are not suitable for use on a flight spacecraft as the probability of zero defects is only 0.522 much below the usually desired 0.999 for pyrotechnic spacecraft devices.

The Poisson distribution is used to determine the probabilities associated with a specified number of failures in the continuum of time. Complex electrical components have been shown to follow the Poisson distribution.

Ten space power speed controllers were tested during the Sunflower development program. The time-to-failure test data is given in table IV.

(a) Write the Poisson failure density and reliability functions.

(b) What is the probability of five failures in 10 000 hours?

(c) What is the probability that 6, 7, 8, 9, or 10 failures will occur or the reliability from the 5^{th} failure?

a. Using the data given in table IV, this problem can be solved as follows:

$$\bar{t} = \frac{\sum_{i=1}^{10} t_i}{N_f} = \frac{8.586 \times 10^4}{10} = 8.59 \times 10^3 \text{ hr/failures}$$

Hence the Poisson failure density function is:

$$f(N_f) = \frac{(t/8.59 \times 10^3)^{N_f}}{N_f!} e^{-t/8.59 \times 10^3}$$

and the reliability function is:

$$R(N_f) = \sum_{j=1}^{10} \frac{(t/8.59 \times 10^3)^j}{j!} e^{-t/8.59 \times 10^3}$$

b. The probability of five failures $f(5)$ in 10 000 hours makes use of the ratio $(t/\bar{t})$. Using this ratio, $f(5)$ becomes

$$\frac{t}{\bar{t}} = \frac{1.0 \times 10^4}{8.56 \times 10^3} = 1.16$$

$$f(5) = \frac{(1.16)^5 e^{-1.16}}{5!} = \frac{2.09 \times 0.314}{1.2 \times 10^2} = 5.47 \times 10^{-3}$$

One easy method to calculate the term $(1.16)^5$ is as follows:

$$\log (1.16)^5 = 5 \log 1.16 = 5(0.148) = 0.740$$

$$(1.16)^5 = 2.09$$

c. The reliability from the 5^{th} to the 10^{th} failure is the sum of the remaining terms in the Poisson expansion. This probability can be calculated using the following equation

$$R(N_f) = \sum_{j=6}^{10} \frac{0.314\ (1.16)^j}{j!}$$

$$R(6) = 0.0013$$

6. Determination of confidence limits

When an estimate is made using discrete distributions, it is expected that additional estimates of the same parameter will be close to the original estimate. It is desirable to be able to determine upper and lower confidence limits at some stated confidence level for discrete distribution estimates. The analytical procedure for determining these intervals is simplified by using specially prepared tables and graphs. Useful tables for the binomial distribution are given in references 5, 8, 9, and 10.

A prior calculation showed that the probability of one defective pyrotechnic unit appearing in a flight quantity of four was 0.37.

What are the upper and lower confidence limits on this estimate at a 90 percent confidence level?

If the number of defectives is r and the confidence level is γ, this problem has the constraints listed below:

$n = 4 \qquad r = 1 \qquad \gamma = 90$ percent

Using these constraints, the upper U and lower L confidence limits

can be obtained from table I in reference 8.

$L = 0.026$

$U = 0.680$

This means that with a 90 percent confidence the probability of one defective bolt appearing in a flight quantity of four is in the interval from 0.026 to 0.680.

The Poisson estimate of reliability from the 5th to the 10th failure for speed controllers was found to be 0.0013 in a previous problem. What are the upper and lower confidence limits on this estimate at a 95 percent confidence level?

The variation in $\overline{t}$ can be found by using Chart I, page 23 from reference 10. Enter Chart I on the 5 percent line at the left hand end of the 5 interval, here $T/\overline{t}_1 = 10.5$; then $\overline{t}_1 = 10\ \overline{t}/T/\overline{t}_1 = 8.57 \times 10^4/10.5 = 8160$ hours. Using the left hand end of the 4 interval $T/\overline{t}_2 = 9.25$; then $\overline{t}_2 = 8.57 \times 10^4/9.25 = 9530$ hours. One easy method to find $Q(5)$ is to use figure 6-1 of reference 5, page 61. The $t/\overline{t}$ ratios of interest are 1.22, 1.16, and 1.05, respectively. For these ratios with $N_f = 5$, the values of $Q(5)$ from figure 6-1 are 0.997, 0.9987, and 0.9992, respectively. Since the sum of the last five terms is desired, $R(5)$ is 0.003, 0.0013, and 0.0008, respectively.

This means that the probability of the 5th to the 10th failure of a speed control occurring is in the interval from 0.0008 to 0.003 at a confidence level of 95 percent.

IV E. Reliability Program Case History

The Lewis Research Center's reliability engineering programs are designed to require:

1. Through planning and effective management of the reliability assurance effort.

2. Definition of the major reliability engineering tasks and their place as an integral part of the design and development process.

3. Assurance of reliability through a complementary program of reliability engineering and evaluation.

1.0 SERT II Reliability engineering

A reliability engineering effort was established and maintained to assure that the complete space system, launch vehicle, spacecraft and associated ground support equipment are capable of meeting the SERT II objectives.

The SERT II design concept is strongly influenced by the philosophy of maximum utilization of previously space qualified hardware, of system redundancy, and of extensive endurance testing of a complete spacecraft under simulated mission conditions. With few exceptions new design is limited to supporting on-board experiments of secondary mission criticality. For all new designs minimum parts derating factors were employed. For newly designed critical components, a review of such factors as complexity, exposure to transients, redundancy, and the scope and depth of the planned test program were used to determine the need for formal stress analysis.

Similar considerations were given to the need for formal failure mode, effect and criticality analysis.

Design review

Formal design reviews conducted by the Project did include participation by R&QAO personnel. The R&QAO did provide an independent appraisal of the design under consideration giving special attention to its reliability performance. These R&QAO representatives did provide follow-up action on items related to reliability areas of concern.

Failure mode, effect and criticality analysis

Projected analyses for newly designed critical systems was developed to determine possible modes of failure and their effect. The primary objective of these analyses was to discover critical failure areas and remove susceptibility to such failures from the system. In the analyses, each potential failure was considered in the light of probability of occurrence and was categorized as to probable effect on mission success of the system to aid in proportioning effort for corrective design action. These analyses were a major consideration in design reviews and also provided an important criterion for test planning.

Reliability modeling

A reliability prediction model was made to show that the system is capable of meeting the specified MTBF goals. Each functional device, input, output, internal and external connection point and boundary was shown in a system block diagram. The model was revised as required by evaluation of the design, design changes, and test data. This model was

used as:

a. A basis for redundancy.

b. A guide for reliability improvements.

c. A guide for failure data reporting and analysis.

Parts and materials selection

The R&QAO did support the Project Office in selection, reduction in number of types, specifications, qualification and application review of parts and materials. R&QAO did review nonstandard parts (i.e., parts selected from sources other than preferred parts lists) and recommend their suitability for use on program hardware.

Stress analysis

Newly designed critical components and subsystems were studied analytically and experimentally to determine the electrical, mechanical and thermal stresses to verify that the designs have adequate derating factors for spacecraft use. Steady state and transient stress were measured. Operating magnitude or shutdown were studied to determine worse case conditions.

In cases where the derating factors cannot be achieved, a derating factor nonconformance list was prepared. This list was reviewed by R&QAO and recommendations for corrective action submitted to the Project Manager.

Electrical

Electrical measurements were made on the developmental model in a laboratory environment. This survey did measure the voltage, current and power for parts operating at over 50 percent of their rating or dissipating more than 0.5 watts.

Thermal

A preliminary thermal survey was conducted on the developmental models in a laboratory environment. This survey did measure the surface or case temperature of each critical or questionable part. A second thermal survey was conducted on the prototype models mounted to demonstrate compliance with flight environmental specifications.

Mechanical

A mechanical survey was conducted on the prototype models mounted to demonstrate proper derating for shock, vibration and acceleration in compliance with flight environmental specifications.

Failure, reporting, analysis and corrective action

An integrated effort was established for failure reporting on tests conducted with flight and prototype hardware and with selected developmental hardware agreed to by the SERT II Project Manager.

Failure reporting

Provisions were established for the organized reporting of failures resulting during selected developmental, acceptance, qualification and life tests, at the component, sub-system and system level. The pertinent information relevant to the failure of the item was furnished to all groups requiring such information.

Failure analysis

The failure analysis of the article was conducted by the appropriate design engineer responsible for the component.

Corrective action resolution

Appropriate corrective action was accomplished on all deficiencies reported on a NASA Failure Report Form. The corrective action was noted as concisely as possible, yet amply detailed, and did denote the required positive action for the resolution of the problem areas.

Review of corrective action activity

Project representatives and R&QAO did jointly participate in periodic engineering review meetings. The purpose of these meetings was to resolve "open" failure and analysis reports, and to define rework, retest, and any additional action necessary to improve and maintain system reliability. A failure, analysis and action report was considered resolved when all concurrence signatures and dates appear in Section IV of the report.

Project summary charts

Dot Diagrams were prepared by the Reliability Office for each sub-system. From these diagrams trouble spots can be readily identified and progress toward their solution observed. The pertinent summary information was transmitted to all interested groups.

Performance goal

This Project used as its performance goal a mean-time between-failures for each sub-system greater than 8 760 hours.

The test data was subjected to weighted statistical analysis to ascertain attainment of the goal by each sub-system.

R&QAO did periodically assess the current progress of each sub-system toward meeting the performance goal.

Equipment log

An equipment log and continuous history on the fabrication, inspection, test, storage and assembly of flight, and prototype components was maintained.

The interested reader can obtain more details on the SERT II reliability and quality assurance provisions and procedures from reference 11.

2.0 Reliability stress analysis of a microthruster power conditioner

Obtaining suitable power-conditioning equipment for electric propulsion units is widely recognized as a critical problem (ref. 12). Data have been accumulated on several electric propulsion research pro-

jects and other power-conditioning development contracts which further show that overstressed electrical parts are a prime cause of equipment failures in electric propulsion experiments.

A typical example of this problem occurred during the WASP fluid dynamic experiment. In this case the failure was in a 28 to 500 volt dc converter which was the power supply for a telemetry transmitter. Failure analysis showed that two, IN 684, subminiature silicon rectifiers had shorted out. Experimental measurements showed that the diodes were not carrying equal amounts of the applied reverse voltage. The other ratings for each diode appeared to be reasonable. The fact that these particular diodes were manufactured with avalanche reverse breakdown properties did not seem to be sufficient protection for long-term, reliable operation under these conditions (refs. 13 to 15).

It is generally recognized that component-part failure rates are increasing functions of the stress applied in operation. Furthermore, it is realized that even the best parts, when operated at maximum-rated stress levels, do not have sufficiently low failure rates to allow the synthesis of highly reliable complex systems. Therefore, the need to derate components in application is clearly established (ref. 16).

Component derating factors are naturally based on the component reliability at various stress levels. Once the necessary component reliability is established, the maximum stress level at which the component could be operated can be determined without violating the reliability requirement. Unfortunately, curves of reliability as a function of stress

exist for only a few components and are generally not well proven even for these. In the remainder of the cases, historical information based on field data obtained from various equipment operating under conditions similar to those of interest must be used.

Table V shows the recommended derating factors for power conditioners This table is based on experimental findings and a survey of the best information currently available. Proper use of these derating factors should yield component failure rates in the range 0.1 to 0.001 percent per 1000 hours. Failure rates will also vary widely for different applications because of the particular circuit's tolerance of component drift. Therefore, to ensure low failure rates the designer should strive to achieve the greatest possible circuit tolerance.

Discussion

An electrical stress analysis test was performed on the microthruster power conditioner while it was operating into an adjustable resistive load bank. (For a more detailed explanation of the apparatus required to operate an ion thruster consult ref. 17). Transient simulation and measurement techniques were worked out. Detailed transient and steady-state data from these measurements are recorded in the microthruster equipment log on file at the Lewis Research Center. These data describe some of the response functions that were observed in the test apparatus under worst-case conditions and help explain why the overstress problems were occurring.

Reliability model

The Lewis microthruster reliability model with the interconnection arrangement of the circuits with the thruster is shown in figure 3. Each solid-line box is a necessary component of the subsystem. The dashed line defines the subsystem boundaries. The power conditioner has 27 circuits that are operated by a dc power source. These circuits change the primary power into the proper voltage and currents for the thruster heaters, the high-voltage electrodes, and signals of thruster parameters.

Each component has been assigned an identification number or letter corresponding to the equation index n or j. Numbers were used to identify main component blocks. Lower-case letters were used for auxiliary components. Two equations have been added to this diagram that describe (1) the theoretical reliability of the thruster equipment and (2) the theoretical reliability of the telemetry circuits. This diagram was used as

(1) A basis for redundancy

(2) A guide for reliability trade-offs

(3) A guide for failure data reporting and analysis

For a more complete treatment of the reliability model consult reference 18.

Summary of findings

A summary of the worst-case electrical stress analysis findings is given in table VI. The parts have been grouped into six categories. The microthruster power-conditioning equipment contained 523 electrical parts; 52 of these parts had not been derated sufficiently to satisfy recommended

derating factors. None of these deficiencies were observed either by calculations or under normal operating conditions. It was necessary to investigate various operating conditions experimentally to find the highest stress conditions. Transients caused by turnon, step changes in parameters, simulated arcs, or turnoff were studied in the laboratory to define these problem areas. Each improper derating condition was analyzed. Corrective design changes were implemented into the breadboard model to eliminate the worst-case overstress conditions.

Although the electrical stress analysis covered the entire microthruster power conditioner, this discussion is limited to one of the more interesting problems, that of the rectifier stresses.

An examination of the data in table VII reveals that ten UTR 62 rectifiers were overstressed. All of these rectifiers were in output indexes 15 and 16 in figure 3. Three IN 649 rectifiers were found to be overstressed in indexes 2, 14, and b in figure 3. One IN 746, two IN 1616, two IN 2999B and eight FD 300 rectifiers were also overstressed, as shown in table VII. In most cases the overstress condition was reverse voltage. In all cases measurements were made for $\pm V$ and $\pm I$ to ensure proper derating under worst-case conditions.

Schematic of index 15

Experimental data for all the electrical parts were obtained by making electrical measurements on the microthruster power-conditioning breadboard. Index 15 for the beam supply is the voltage quadrupler circuit shown schematically in figure 4. The input forcing function

$V_{1,i} = V_{2,i}$ is a regulated -24 volts dc. This voltage is applied through an inverter alternately to each half of the primary of T9. The stepped-up output $V_{5,o}$ of T9 is used to charge four quadrupler capacitors, C_{58} to C_{62}, connected through the rectifiers, CR_{97} to CR_{112}, to generate +1600 volts dc output, $V_{6,o}$ (Ref. 19). The table in figure 4 shows the final trim capacitance values that were used in the stress-relieved beam supply.

The UTR 62 rectifiers are alloy-diffused silicon devices. The fabrication process is controlled in such a manner as to optimize recovery time. Fast recovery time suggests that an abrupt junction model is appropriate for these devices. This model is used later to show why proper derating for reverse voltage (-V) is important for long-term reliability.

Test apparatus

The Major piece of test equipment used for these observations was an oscilloscope. One of the more interesting test apparatus setups used to measure rectifier voltage is shown in figure 5. A 200 to 1 attenuator and voltage isolation probe was connected to the test specimen. A logarithmic-scale compression circuit was used to measure the rectifier voltages because of its dynamic range of 4 orders of magnitude. The circuit was sensitive to test apparatus loading. The differential probe had an input impedance of 30 megohms and 3 picofarads, which appeared to give minimum circuit disturbance. The signal ratio V_{max}/V_{min} was reduced from 600/0.8 to 3/0.004 by the probe.

This information is amplified by a factor of 10 to 30/0.04 and fed into logarithmic amplifiers for compression. The voltage across the test specimen was obtained by subtracting channel B from channel A. The display device was the oscilloscope.

Ground-loop noises were reduced by connecting the oscilloscope common with the power-conditioner-circuit common and isolating the oscilloscope from its power source.

Unbalance and zero drift are critical adjustments in this dc-coupled measurement technique. Proper attention must be given to each component to assure that it is calibrated, operating, and adjusted properly. Connecting channels A and B to the same point, as a check, assures cancellation of unwanted or interfering signals. It is difficult to resolve $\pm V$ beyond about ± 10 percent because of scale compression. However, for dynamic measurements on a system with this complexity, greater accuracy was not required.

Experimental data

Electrical stresses for rectifiers CR_{97} to CR_{112} at laboratory ambient temperature are shown in table VIII. The data show that $+V$, $+I$, and W meet the requirements of table V. The measured data at laboratory ambient temperature (approx. 21° C) are compared with the specified spacecraft heat sink at a maximum of 60° C to obtain the component derating factor for these conditions. Some of the rectifier diodes have reverse voltage and current stresses, $-V$ and $-I$, with derating factors of 1.0 and 12.5, respectively, which is considerably above the specified deratings.

A P-N junction is reverse recovered from the forward conducting state when the current passing through the junction goes to zero (i.e., righthand thermally generated hole current I_{gp} equals lefthand thermally generated electron current I_{gn}). For a more complete treatment of the theory of P-N junctions consult references 20 and 21. The junction current goes to zero by diffusion and drift, removing the majority carriers from the junction. At the instant of switching, a current spike occurs which was the cause for $|-I|$ to exceed its dc rating by a factor of about 10. The energy rating of the rectifier is not exceeded by these repetitive reverse-current spikes and is, therefore, not a major concern.

Table VIII also shows that the junctions were not sharing reverse voltage equally. The appendix reviews the current theory applicable to junction breakdown to show that equal -V sharing is important for rectifier reliability. For example, CR_{100} would hold off a potential of 600 volts while CR_{98} was carrying only 30 volts peak. Based on these observations, it was clear that reliability could be improved if the diodes shared the reverse voltage more equally. In our example, CR_{97} would pick up about five times more -V when CR_{100} shorted out than if CR_{98} shorted out. After a time CR_{97}, which no longer would be properly derated, could fail by this same junction deterioration phenomenon and thereby cause CR_{98} and CR_{99} to carry the remaining burden with no derating. Eventually all rectifiers would fail and the power-conditioner output would go to zero.

Most probably the part with the greatest electrical stresses will fail first. Past experience with diodes has shown that shorting is the dominant failure mode. If some method could be found to make all reverse potentials nearly equal, a derating factor of about 0.33 could be achieved, and the probability of junction deterioration breakdown occurring could be reduced.

Conventional methods (refs. 14 and 15) were employed to improve reverse-voltage sharing as this could possibly have improved the long-term reliability of a series of rectifiers. The circuit stopped operating properly when these different methods were tried.

Recognizing that equal C_j terms should share $-V$ equally, three fixed trim capacitors were added to each string to meet the desired constraint $|0.9\ V| \leq |-V| \leq |1.1\ V|$. In figure 4 the arrangement of trimmer capacitors and their values are shown. Table IX shows that quite an improvement in $-V$ has been accomplished by adding the proper C_t without affecting $-I$ appreciably. The maximum spread on uncompensated reverse voltage of 17 to 600 volts peak has been reduced to 160 to 205 volts peak (compare table VIII with table IX).

Reverse voltage may have exceeded the desired tolerance by a small amount; however, the tolerance was primarily determined by the fixed values of mica capacitors available. Reverse current has been increased roughly by a factor of 2. This is not nearly enough to influence the energy rating W or circuit operating parameters. It remained to show that temperature would not adversely influence voltage sharing and that such a rectifier string would operate for a long time without failure.

Temperature data for $\pm I$ and $\pm V$ were taken by placing the rectifiers, CR_{97} to CR_{112}, and trim capacitors C_t in a temperature chamber. Ten temperatures spaced approximately 14° C apart in the range from -54° to 85° C were selected as test points. The test data for $\pm I$ and $\pm V$ does not show that temperature has any pronounced effect on the circuit response. Table IX summarizes the data for $-V$ by giving the central value $-\bar{V}$, and standard deviation σ, in the test temperature range.

The mean value of reverse voltage varies from 162 with $\sigma = 7.7$ volts peak to 209 with $\sigma = 5.8$ volts peak. Further consideration of figure 4 helps explain why temperature has not much influence on voltage sharing for this compensation method. The transformer T9 has been optimized for weight, which tends to increase copper losses; copper, silicon, and mica all have positive changes in resistance, leakage, and capacitance, with temperature. When these two facts are considered, one explanation for this nominal temperature effect may be that as temperature increases the copper losses increase. At the same time the load impedance is decreasing, which tends to maintain a constant response function. Conversely, when temperature decreases the copper losses decrease and the load impedance increases, which tends to hold $V_{6,o}$ constant.

Exhibited response

The microthruster power-conditioning breadboard revised to eliminate high-stress areas was run in the laboratory without failure for 7052.3 hours.

Conclusions and recommendations

The worst-case electrical stress analysis test performed on a microthruster power-conditioning breadboard disclosed a number of electrical parts which were overstressed. Each overstressed part was analyzed to determine suitable corrective action. Corrective design changes were implemented into the breadboard model.

Experimental measurements showed that a worst-case stress analysis obtained through laboratory testing is necessary to identify over-stressed conditions which are not evident from an analytical study or from subjecting the equipment to normal operating conditions. The rectifier diode problem is an example of a worst-case stress condition that was identifiable only through laboratory testing. As a result of this testing, the rectifier problem was solved by adding high-reliability mica capacitors across the rectifiers to improve the voltage sharing capabilities of this design.

Breakdown theory shows that junction deterioration could have been the cause of several critical failures which have occurred on past ion-engine research projects. A further review of these breakdown theories showed that avalanche construction is not always the answer to obtaining long-term reliable operation under a repeated transient condition.

An ion-thruster power conditioner was modified to eliminate the evidenced over-stressed conditions described herein. This power conditioner operated properly for more than 7000 hours.

APPENDIX - Junction Breakdown

Presently there are two theoretical explanations as to how a P-N junction which has voltage applied in the reverse direction abruptly changes from high resistance to essentially zero. Figure 6 shows these two types of breakdown. Both types of breakdown have been observed on an oscilloscope in the laboratory.

From the origin to point A, I appears to be following the theoretical diode equation (ref. 20),

$$I = I_S\left[\exp\left(\frac{qV}{kT} - 1\right)\right] \qquad (1)$$

and

$$I_S = I_{gp} + I_{gn}$$

From A to B, I is increased by a leakage component. From B to E, there are two apparent paths by which breakdown occurs. These paths B-C-E and B-D-E are sometimes referred to as the zener and Townsend breakdown paths, respectively. The actual breakdown mechanisms are not well understood as each theory does not fit exactly with the observed phenomena.

The zener breakdown theory (ref. 22) postulates that the covalent bonds in the vicinity of the depletion are spontaneously disrupted by the high electric fields that exist in this region. The carriers made available by the disrupted bonds would add to I_{gp} and I_{gn}. For

high fields, large number of field carriers would be generated, limited only by the external circuit resistance, taking I into the E-F or avalanche region (refs. 23 and 24).

High fields are certainly present in P-N junctions under reverse bias conditions, as can be seen from the following simplified analysis. The experimentally studied rectifiers were UTR 62 devices with fast recovery time. Figure 7 shows an abrupt junction model which is appropriate for these devices. Since $x = W_1 + W_2$ and $\xi = 0$ (fig. 7), a point of inflection occurs at $x = 0$ and ξ is maximum (see ref. 20); therefore,

$$\xi_{max} = \frac{qN_d}{\epsilon} W_2$$

For an abrupt junction,

$$\xi_{max} = \left(\frac{2V_B}{\epsilon \mu_n P_n}\right)^{1/2}$$

For silicon this becomes,

$$\xi_{max} \simeq 6.3 \times 10^4 \left(\frac{V_B}{P_n}\right)^{1/2} \qquad (2)$$

where

$$P_n = 5.0\ \Omega\text{-cm}$$

$$V_B = V_{eq} - V, \qquad V_{eq} \ll V$$

Therefore,

$$V_B \simeq |-V| = 200 \text{ volts}$$

and

$$\xi_{max} = 3.98 \times 10^5 \text{ volts/cm}$$

Even though this analysis is only approximate, it is clear that this is a very high field and spontaneous disruption of the covalent bonds is quite likely. However, due to the inability of this theory to explain some observable phenomena, it is no longer accepted as complete.

The Townsend breakdown theory (ref. 25) develops the analog between a gas discharge and a P-N junction breakdown. The reverse junction current is composed of thermally generated holes, electrons, and leakage (eq. (1) and fig. 6). When the applied junction potential is increased, from point B, -V increases the energy state to a point where the thermal carriers begin to experience ionizing collisions. Each ionizing collision contributes secondary holes and electrons to -I, beyond the leakage contribution. This causes carrier multiplication to occur, as each ionized carrier may strike several atoms as it passes through the depletion zone. Depending on the magnitude of the applied potential -V, the number of ionizing collisions can cascade quite rapidly as shown along the path B-D-E (fig. 6). From point E upward, the number of carriers generated by collision is no longer a function of -V, as V_A has been reached. The junction current is,

in the E-F region, again, only limited by the external circuit resistance.

It can be seen that all P-N junctions will avalanche at some potential. Whether this disturbance occurs along path B-D-E or B-C-E does not change the fact that this is a very high stress condition for any junction and can easily cause failure. It has been shown in the literature (refs. 13 to 15) that the instantaneous energy rating cannot be exceeded, or sudden failure by punch-through will occur. The fact that a particular P-N junction can operate in the E-F region under controlled conditions by virtue of avalanche construction does not give total assurance against deterioration due to repeated high reverse-voltage stresses.

Elevating the temperature in which the junction operated aggravates the situation still further. Temperature causes I_S to increase. For silicon, I_S increases about 1 order of magnitude for each 20 K. This increase would suggest that since the number of carriers has increased, the avalanche potential V_A should decrease. Here, both theories appear to be misleading, as in many cases the measured value of V_A increases slightly with temperature.

It appears that the Early effect (ref. 26) under certain conditions may cause deterioration in P-N junctions. This may explain why P-N junctions that were avalanche protected still suffered gradual deterioration as a result of high reverse-voltage stress. This potentially unreliable condition can be minimized by adding a small trimmer capacitor across each exposed junction to cause equalization of reverse voltage.

REFERENCES

1. Anon.: Reliability Theory and Practice. ARINC Res. Corp., Washington, D.C., 1962.

2. Anon.: Reliability by Design. General Electric Co., Defense Elec. Div., Waynesboro, Va., 1964.

3. Bazovsky, Igor: Reliability Theory and Practice. Prentice-Hall, Inc., 1961.

4. Lalli, V. R.: "Reliability Testing and Demonstration," presented at the Sixth Annual Reliability Engineering and Management Institute, Univ. Arizona, Tucson, Ariz., Nov. 5-7, 1968.

5. Calabro, S. R.: Reliability Principles and Practices. McGraw-Hill Book Co., Inc., 1962.

6. Hoel, Paul G.: Elementary Statistics. John Wiley & Sons, Inc., 1960.

7. Anon.: Failure Distribution Analyses Study. Vols. I, II, and III. Computer Applications, Inc., Aug. 1964.

8. Lochner, R. H.: Estimation and Prediction Using the Binomial Distribution. Reliability Res. and Ed. Dept., General Motors Corp., Milwaukee, Wisc., 1963.

9. Leone, F. C., et al.: "Percentiles of the Binomial Distribution," Case Inst. Tech., Cleveland, Ohio, 1967.

10. Lochner, R. H.: Reliability Calculations for Exponential Population. Reliability Res. and Ed. Dept., General Motors Corp., Milwaukee, Wisc., 1963.

11. Anon.: SERT II Reliability and Quality Assurance Manual. R & QA Office, NASA Lewis Research Center, Cleveland, Ohio, 1968.

12. Anon.: Propulsion. Space/Aeronautics, Res. & Dev. Tech. Handbook, vol. 44, no. 2, 1965-66, p. 49.

13. Hitchcock, R. C.: Avalanche Diodes: The Answer to High PRV. Electronic Design, vol. 12, no. 17, Aug. 17, 1964, p. 166.

14. Gutzwiller, F. W.: Rectifiers in High Voltage Power Supplies. Electronic Design, July 23, 1958.

15. Von Zastrow, E. E.: Voltage Failures in Series-Connected Diodes - Their Cause and Prevention. Electronic Design, vol. 13, no. 22, Oct. 25, 1965, p. 62.

16. Anon.: JPL Preferred Parts List - Reliable Electronic Components. Spec. ZPP-2061-PPL-H. Jet Propulsion Lab., Calif. Inst. Tech., July 1, 1966, table VI.

17. Kotnik, J. Thomas; and Sater, Bernard L.: Power-Conditioning Requirements for Ion Rockets. Presented at the IEEE International Conference and Exhibit on Aerospace Electro-Technology, Phoenix, Arizona, Apr. 19-25, 1964.

18. Lalli, Vincent R.: Ion Engine Subsystem Reliability Procedure. Presented at the IEEE, IES, and ASQC Eleventh National Symposium on Reliability and Quality Control, Miami Beach, Florida, Jan. 12-14, 1965.

19. Smith, Fritz L., ed.: Radiotron Designer's Handbook. Fourth ed., Radio Corp. of America, 1953.

20. DeWitt, David; and Rossoff, Arthur L.: Transistor Electronics. McGraw-Hill Book Co., Inc., 1957.

21. Shockley, W.: The Theory of P-N Junctions in Semiconductors and P-N Junction Transistors. Bell System Tech. J., vol. 28, no. 3, July 1949, pp. 435-489.

22. McAfee, K. B.; Ryder, E. J.; Shockley, W.; and Sparks, M.: Observations of Zener Current in Germanium P-N Junctions. Phys. Rev., vol. 83, no. 3, Aug. 1, 1951, pp. 650-651.

23. McKay, K. G.; and McAfee, K. B.: Electron Multiplication in Silicon and Germanium. Phys. Rev., vol. 91, no. 5, Sept. 1, 1953, pp. 1079-1084.

24. McKay, K. G.: Avalanche Breakdown in Silicon. Phys. Rev., vol. 94, no. 4, May 15, 1954, pp. 877-884.

25. Cobine, James D.: Gaseous Conductors, Theory and Engineering Applications. Dover Publications, 1958.

26. Early, J. M.: Effects of Space-Charge Layer Widening in Junction Transistors. Proc. IRE, vol. 40, no. 11, Nov. 1952, pp. 1401-1406.

TABLE I. - TEST DATA FOR A MECHANICAL PART

Ordered sample number	t_f, K hr	t_f^2, $(K\ hr)^2$
1	60	3600
2	65	4225
3	68	4624
4	70	4900
5	75	5625
6	75	5625
7	80	6400
8	83	6889
9	85	7225
n = 10	90	8100
Totals	750	57 213

TABLE II. - CABLE TIME-TO-FAILURE DATA

Ordered sample number	Time-to-failure, hr	Median rank[a]	5% Rank[a]	95% Rank[a]
1	1 100	6.7	0.5	25.9
2	1 890	16.2	3.7	39.4
3	2 920	25.9	8.7	50.7
4	4 100	35.5	15.0	60.7
5	5 715	45.2	22.2	69.7
6	8 720	54.8	30.3	77.8
7	12 000	64.5	39.3	85.0
8	17 500	74.1	49.3	91.3
9	23 900	83.3	60.6	96.3
n = 10	46 020	93.3	74.1	99.5

[a]From tables 2, 5, and 15 of reference 7.

TABLE III. - PASCAL'S TRIANGLE

FOR BINOMIAL COEFFICIENTS

Sample size	Possible failure	Binomial coefficients
1	2	1
2	3	1 2 1
3	4	1 3 3 1
n = 4	5	1 4 6 4 1

TABLE IV. - SPEED CONTROLLER

TIME-TO-FAILURE DATA

Ordered sample number	Time-to-failure, hr
1	3 520.0
2	4 671.2
3	6 729.3
4	7 010.0
5	8 510.2
6	9 250.1
7	10 910.0
8	11 220.5
9	11 815.6
10	12 226.4
Total	85 866.3

TABLE V. -COMPONENT DERATING FACTORS FOR POWER CONDITIONERS

Component	Derating factor[a]	Component derating weighting factors		Stress	Remarks
		X	Y		
Capacitors				Voltage	The following equation establishes the derating factor for capacitors where values of X and Y are given: Derating factor = $X - \frac{C - C_{min}}{C_{max} - C_{min}} (Y)$ where C capacitance value of capacitor for which derating factor is desired; C_{min} smallest capacitance value available with same case size and voltage rating as C; C_{max} largest capacitance value available with same case size and voltage rating as C
Ceramic disc	0.7	---	---		
Ceramic, low voltage	---	0.5	0.2		
Glass:					
CYFR10 and CYFR15	0.7	---	---		
CYFR20 and CYFR30	.5	---	---		
Porcelain	---	0.7	0.2		
Mica	---	.7	.2		
Plastic film	---	.5	.2		
Paper	---	.8	.1		
Metalized	---	.5	.2		
Tantalum, solid	---	.7	.3		
Tantalum, wet slug and foil	0.7	---	---		
Connectors, low voltage	---	---	---	Current	Contacts shall be derated to 75 percent of rating for individual contacts. The average current rating from 1 to 15 contacts shall be decreased linearly to 20 percent. For more than 15 contacts the rating is 20 percent of the normal individual contact rating. The applied voltage between contacts or between contacts and shell shall not exceed 250 volts rms.
Silicon diodes					Current and voltage derating factors shall be applied simultaneously.
Signal and switching	0.6	---	---	+I	
	.5	---	---	+V, -I	
	.3	---	---	$\overline{W}$	
Power ($I_o \leq 10A$)	.85	---	---	+I	
	.5	---	---	+V, -I	
	.43	---	---	$\overline{W}$	
Power ($10A < I_o \leq 35A$)	.75	---	---	+I	
	.5	---	---	+V, -I	
	.38	---	---	$\overline{W}$	
Zener (power ≤ 1W)	.5	---	---	Power	
Zener (1W < power ≤ 50W)	.5	---	---	Power	
Microcircuits	---	---	---	-------	Supply voltages may be reduced to effect lower power consumption, at the price of slower switching speeds and narrower noise-immunity margins. Allowable fan-out should be reduced for reliable operation. Operation over wide temperature ranges will generally result in decreased circuit margins and fan-out capability. Operational stability may be improved if power-supply voltage tolerances are tightened, especially if the devices employ non-saturating circuitry.
Relays	0.3	---	---	Current	----------
Resistors				Power	----------
Composition	0.7	---	---		
Film	.4	---	---		
Wirewound power	.5	---	---		
Wirewound precision	.4	---	---		
Transformers	0.4	---	---	Power	----------
Silicon transistors	.25	---	---	Power	Voltage applied across any junction or group of junctions shall not exceed 50 percent of rated voltage.

[a]Derating factor = $\frac{\text{Maximum stress for reliable operation}}{\text{Rated stress}}$

TABLE VI. - SUMMARY OF WORST-CASE

ELECTRICAL STRESS ANALYSIS

RESULTS

Component	Total used	Overstressed[a]
Rectifiers	167	26
Transistors	84	9
Capacitors	91	10
Resistors	170	2
Transformers	9	4
Relays	2	1
Total	523	52

[a]Percentage of parts overstressed, 9.9 percent.

TABLE VII. - OVERSTRESSED-RECTIFIER DETAILS

Rectifier, CR	Derating factor[a]	Type	Index (fig. 1)
81, 84, 101	0.80	UTR 62	16
85	1.08	↓	16
89, 93	.93	↓	16
100, 108	1.00	↓	15
109	.63	↓	15
112	.73	↓	15
7	.97	IN 649	2
22	1.74	↓	b
37	5.18	↓	14
113, 114	Spikes	IN 1616	10
54	.97	IN 746	17
8, 9	.79	IN 2999B	10
14, 15	Spikes	FD 300	4
134, 135, 137	↓	↓	11
146, 147	↓	↓	8
165	↓	↓	2

[a]The specified derating factor for working inverse voltage as given in table I is 0.50.

TABLE VIII. - EXPERIMENTAL CIRCUIT DATA AT LABORATORY AMBIENT TEMPERATURE (21° C)

Rectifier, CR	Rating at 60° C				
	600	1.1 at 1A	1600	0.07 at 600 V	105
	Reverse voltage, -V, volts	Voltage, V, volts	Current, I, mA	Reverse current, -I, mA	Energy rating, W, watt-sec
97	62	0.59	3.8	0.9	0.14×10^{4}
98	30	↓	↓	↓	.07
99	56	↓	↓	↓	.13
100	600	↓	↓	↓	1.4
101	480	.63	8.0	↓	1.1
102	48	↓	↓	↓	.11
103	52	↓	↓	↓	.12
104	240	↓	↓	↓	.55
105	40	.69	20.0	0.8	.08
106	17	↓	↓	↓	.03
107	28	↓	↓	↓	.06
108	600	↓	↓	↓	1.2
109	380	↓	17.0	↓	.76
110	64	↓	↓	↓	.13
111	58	↓	↓	↓	.11
112	440	↓	↓	↓	.88

TABLE IX . - COMPENSATED, EXPERIMENTAL,

RECTIFIER DATA

Rectifier, CR	Temperature, °C			
	21		-54 to 85	
	Reverse voltage, -V, peak volts	Reverse current, -I, peak mA	Mean reverse voltage, $-\bar{V}$, peak volts	Standard deviation, σ, peak volts
97	205	1.7	209	5.8
98	200	↓	195	4.7
99	175	↓	172	5.8
100	205	↓	209	4.7
101	190	1.6	195	4.7
102	178	↓	173	7.7
103	170	↓	179	7.7
104	190	↓	198	7.1
105	160	↓	171	7.7
106	162	↓	172	5.8
107	180	↓	183	4.7
108	190	↓	196	5.8
109	192	1.4	201	4.7
110	165	↓	169	4.7
111	160	↓	162	7.7
112	175	↓	179	7.1

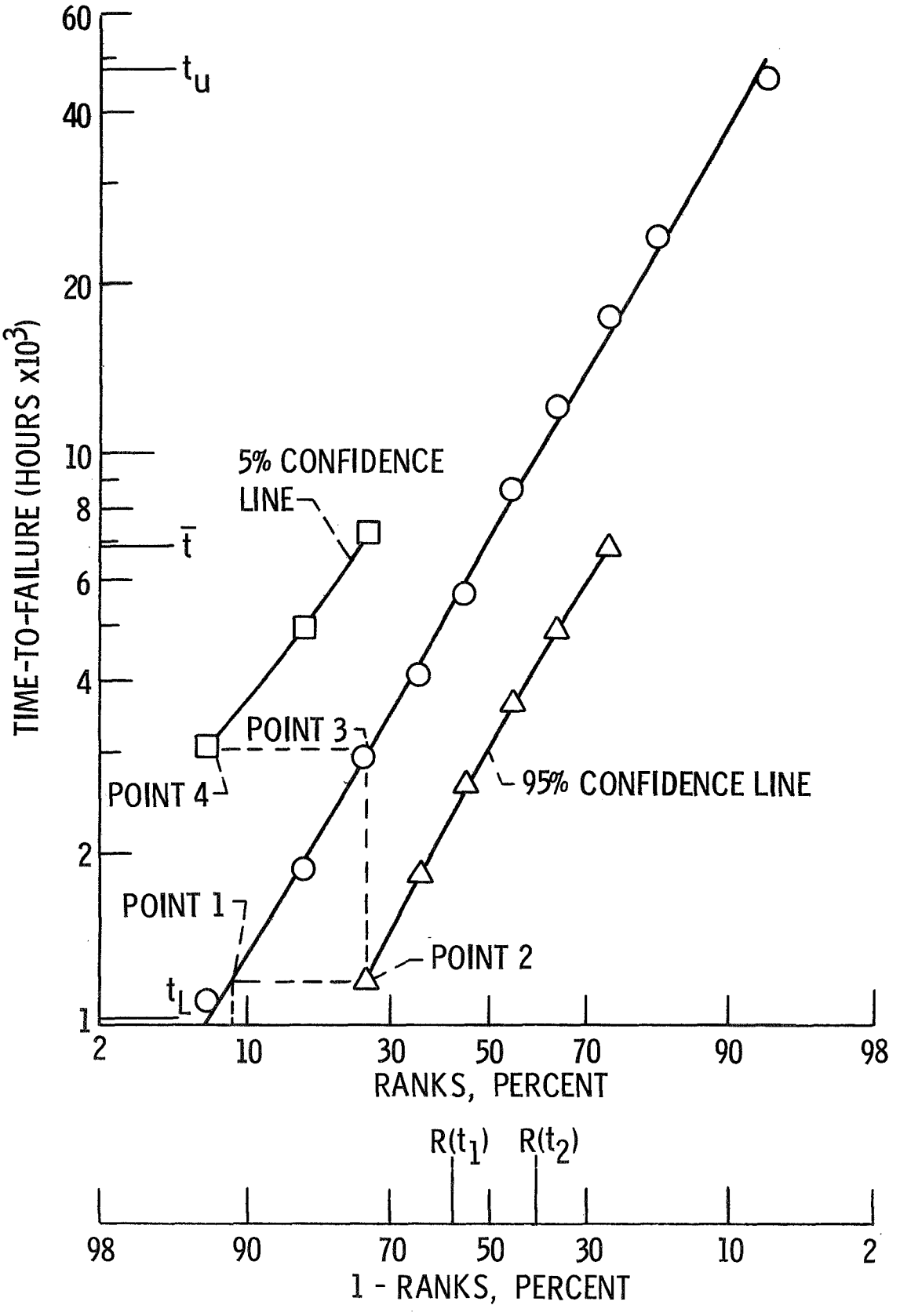

Figure 1. - Lognormal life test diagram.

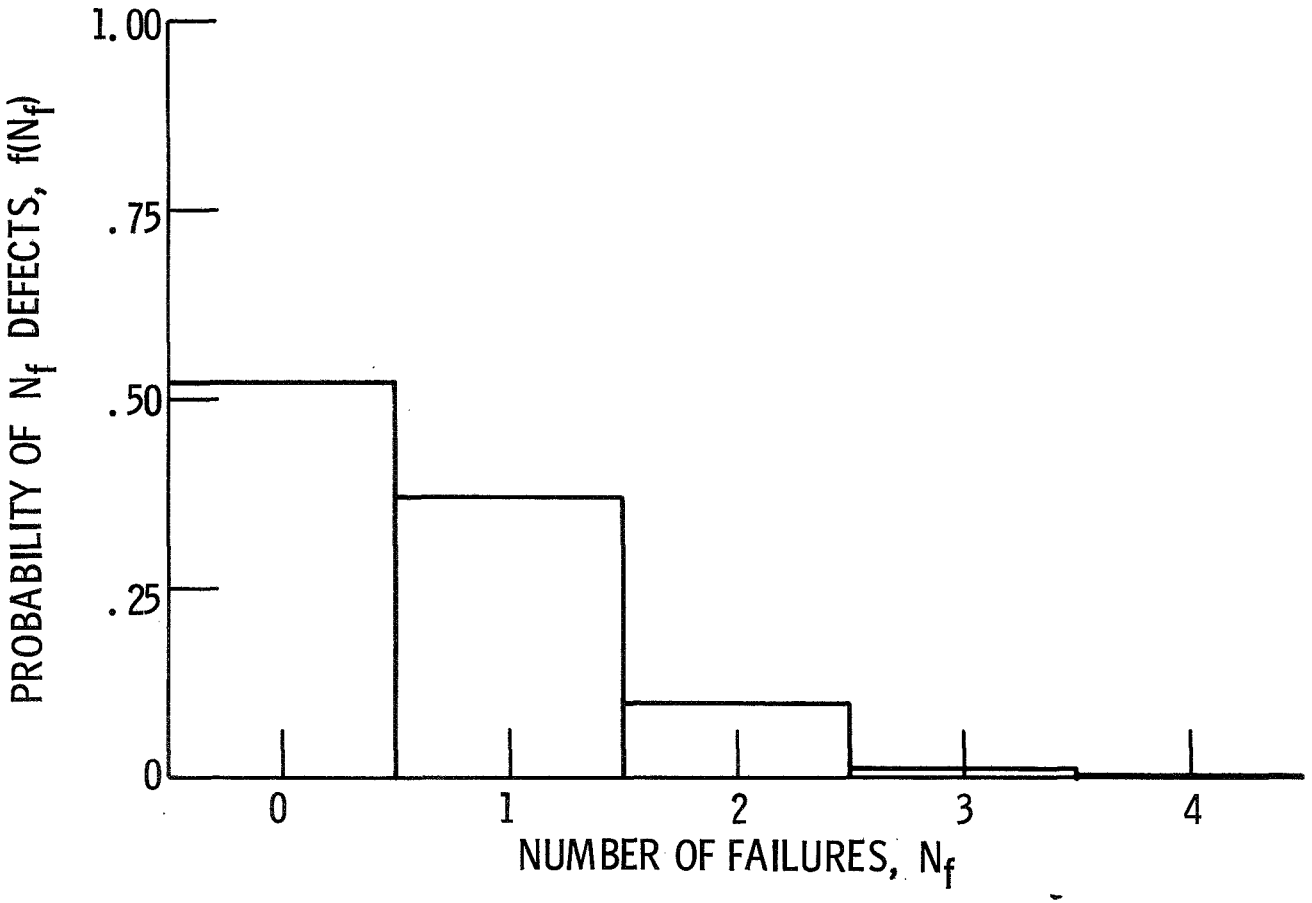

Figure 2. - Explosive bolts histogram.

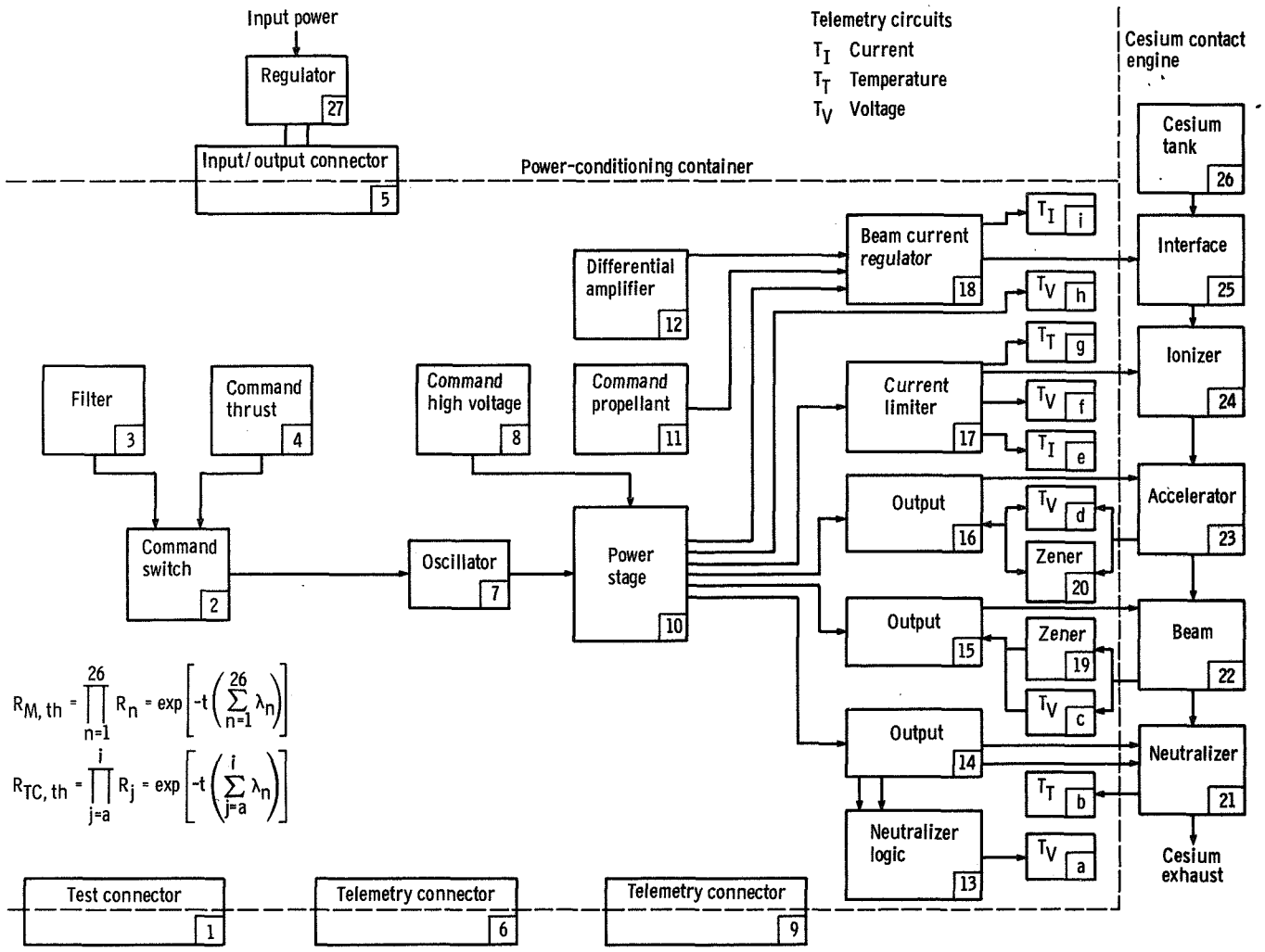

Figure 3. - Microthruster reliability model with identifying devices.

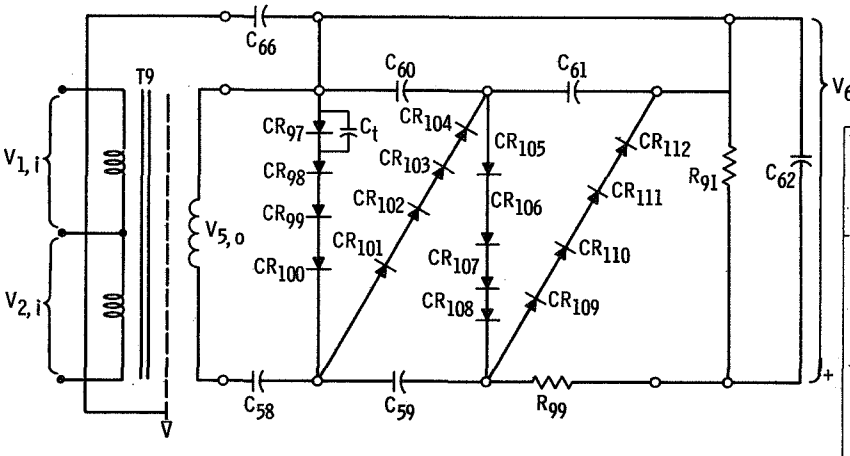

Rectifiers, CR	Trimmer capacitance, C_t, pF
97	27
98	0
99	54
100	156
101	156
102	30
103	0
104	45
105	24
106	0
107	45
108	150
109	72
110	0
111	5
112	60

Figure 4. - Index 15. Output voltage, 1.6 kilovolts dc; maximum output rectifier current, 3.0 milliamperes dc; frequency, 2 kilohertz; input potential, 24 volts dc; $\theta_{1,i} = -\theta_{2,i}$.

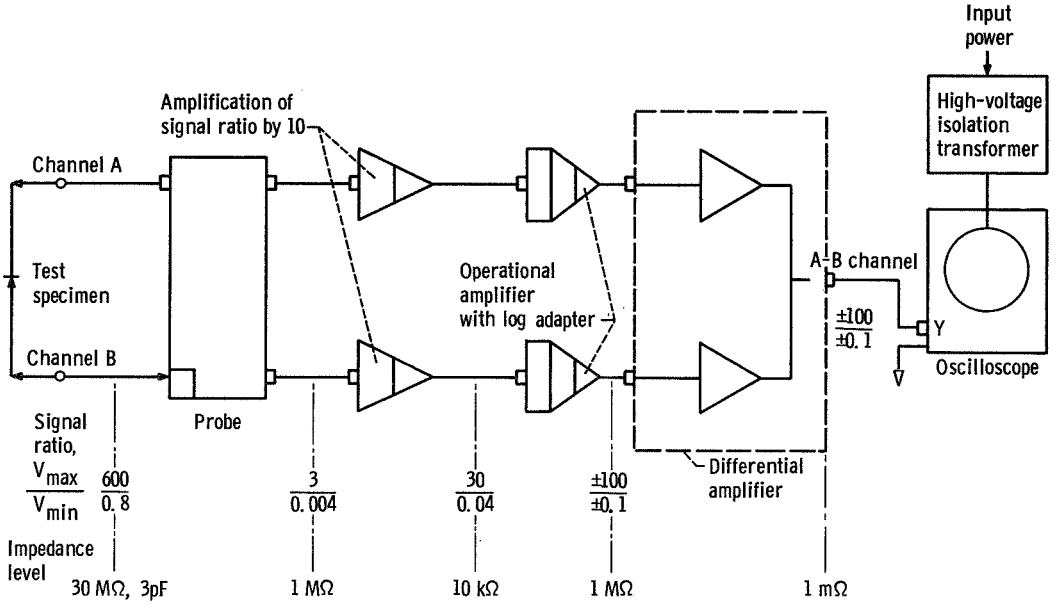

Figure 5. - Apparatus setup for rectifier voltage.

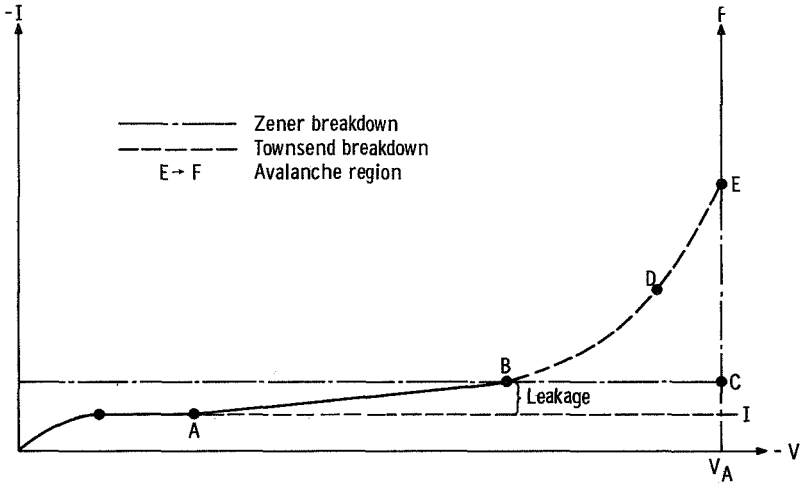

Figure 6. - Steady-state junction breakdown.

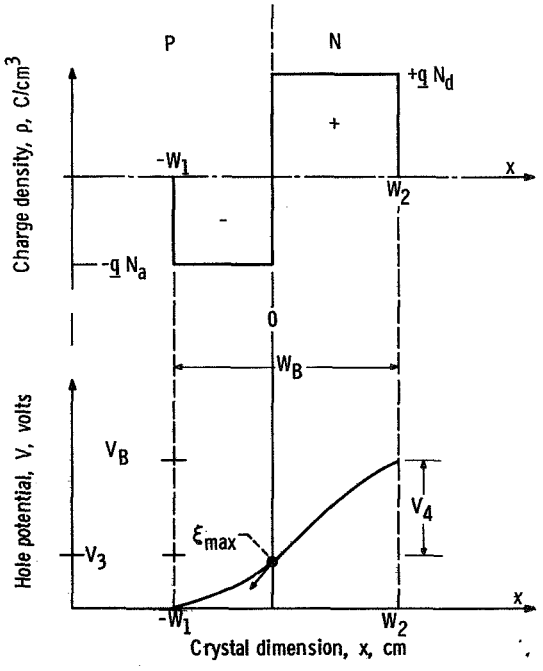

Figure 7. - Abrupt junction model.